

DualMem: Bypassing the Objectness Bottleneck for Calibrated Unknown-Stream Filtering in Open-World Object Detection

Yingjun Xiao¹, Xi Chen², Gang Fang^{3*}, Siyuan Chen²

¹School of Artificial Intelligence, Guangzhou University, Guangzhou, China

²School of Computer Science and Cyber Engineering, Guangzhou University, Guangzhou, China

³Institute of Computing Science and Technology, Guangzhou University, Guangzhou, China

Abstract

Open-world object detection (OWOD) requires detectors to localize known classes and flag unknown objects for future incremental learning. We observe that the unknown prediction streams of strong OWOD detectors are heavily polluted: across PROB, OW-DETR, and HypOW on M-OWODB, future-task positive unknowns account for less than 10% of unknown predictions, while background false positives occupy 46–71%. We show this is not a missing-information problem but an *information bottleneck* at the objectness head: on PROB Task 1, a linear probe on the 256-D decoder query reaches AUROC = 0.908 for positive-versus-negative unknown discrimination, while the final one-dimensional objectness scalar drops to 0.642. A frozen SigLIP feature, with no access to the detector, independently restores most of this proposal-level separability at the filtering stage (AUROC = 0.871). Motivated by this, we propose DualMem, a calibrated post-hoc filter that assumes a small image-disjoint annotated calibration split for held-out future-task objects and performs a *non-parametric likelihood ratio test* in the frozen SigLIP feature space. It uses a *k*-nearest-neighbor positive memory to guard future-task objects and a negative memory to suppress background-like proposals. The decision threshold is selected by Neyman–Pearson calibration, exposing an explicit, user-controllable trade-off between false-unknown suppression and novel recall. Across PROB, OW-DETR, and HypOW on M-OWODB Task 1, DualMem reduces background-type false unknown proposals per image by 44.9%–66.3% (mean 56.6%). On PROB Task 1, it more than doubles the reduction achieved by a natural K-means prototype baseline, while leaving known-class mAP unchanged because known detections bypass the filter.

1 Introduction

Open-world object detection (OWOD) asks a detector to operate beyond a fixed label set: it must localize known classes, flag unknown objects, and later incorporate these unknowns through incremental learning. Recent OWOD detectors have made steady progress on unknown recall, from early open-world formulations to DETR-style, probabilistic, hyperbolic, and prototype/cascade variants (Joseph et al. 2021; Carion et al. 2020; Gupta et al. 2022; Zohar, Wang,

*Corresponding author.



Figure 1: Motivation. The unknown prediction stream of a strong OWOD detector is dominated by non-novel outputs. On PROB Task 1, only 9.1% of unknown predictions are positive unknowns, while most predictions are background false positives or known objects predicted as unknown.

and Yeung 2023; Doan et al. 2024; Wu et al. 2022; Ma et al. 2023; Yu et al. 2022). Yet a closer look at what these detectors actually output reveals a structural problem: the unknown prediction stream is heavily polluted by detections that are not future-task objects.

We decompose the unknown stream into four categories: positive unknowns, which match future-task ground-truth objects; negative unknowns, which do not match any ground truth; known-as-unknown predictions, which overlap current known objects; and ambiguous predictions. Figure 1 illustrates this decomposition for PROB on M-OWODB Task 1. Although PROB is a strong OWOD detector, only 9.1% of its unknown predictions on the val2017 split are positive unknowns, while 46.3% are negative unknowns and 23.9% are known objects mislabeled as unknown. This pattern is not specific to PROB: across PROB, OW-DETR, and HypOW, positive unknowns account for less than 10% of the unknown stream in all nine detector-task cells from Task 1 to Task 3. Thus, the practical challenge is not only to recall unknown objects, but also to clean a prediction stream dominated by non-novel outputs.

Why do detector outputs fail to separate positive and negative unknowns? A natural explanation is that the detector may simply lack the information needed for this distinction. Our analysis shows the opposite. On PROB Task 1, the detector’s final objectness score achieves only AUROC = 0.642 for positive-vs-negative unknown discrimination, indicating weak separability at the output. However, a linear

probe trained on the detector’s 256-D decoder query features reaches AUROC = 0.908 ± 0.009 under five-fold cross-validation. The information needed to distinguish positive from negative unknowns exists inside the detector, but it is largely lost when the decoder query is compressed into a one-dimensional objectness scalar. A frozen SigLIP ViT-B/16 crop feature, with no access to the detector’s internal state, achieves AUROC = 0.871 ± 0.013 , recovering much of the lost discriminability from an external representation. These results identify the objectness head as an information bottleneck: the detector contains useful evidence, but its final unknown confidence signal discards it.

This observation motivates DualMem, a post-hoc unknown-stream filter that treats the OWOD detector as fixed and applies a non-parametric likelihood ratio test in the frozen SigLIP feature space. Two memories—a positive memory of future-task proposals and a negative memory of background false positives—define class-conditional kernel density estimators built directly on calibration features (k -nearest neighbor; no centroid quantization). The decision threshold is selected by Neyman–Pearson-style calibration to target a novel mis-suppression budget α , turning an opaque magic number into an explicit precision–recall trade-off. Across three architecturally distinct detectors—PROB, OW-DETR, and HypOW—DualMem reduces FUPI by 56.6% on average (range 44.9–66.3%), with U-Recall preserved within 3.4 percentage points and known-class mAP unchanged because known detections bypass the filter. We deliberately choose the minimal post-hoc construction—no detector retraining, no new losses—so that any improvement can be attributed to bypassing the scalar objectness bottleneck and restoring proposal-level separability at the filtering stage.

Our contributions are threefold:

- **Diagnosis: scalar objectness is a cross-detector bottleneck.** Across PROB, OW-DETR, and HypOW on M-OWODB Task 1, the final objectness scalar is a weak positive-vs-negative unknown discriminator, with AUROC 0.642, 0.526, and 0.516, respectively, and high positive/negative overlap. In contrast, detector-internal proposal features achieve AUROC 0.908, 0.855, and 0.881, while frozen SigLIP crop features achieve AUROC 0.871, 0.828, and 0.888. These results show that the unknown stream is not merely information-poor; rather, discriminative proposal-level information is not exposed by the final one-dimensional objectness interface.
- **Method: DualMem as a minimal post-hoc bypass of the objectness bottleneck.** We treat unknown-stream filtering as a non-parametric likelihood ratio test in a frozen SigLIP feature space. Two k -nearest-neighbor memories—one for positive unknowns, one for background—define class-conditional density estimators; the suppression threshold is selected by Neyman–Pearson calibration to target the false-suppression rate at a user-specified α . On M-OWODB Task 1 with $\alpha = 0.10$, this reduces FUPI by 58.6% on PROB, 44.9% on OW-DETR, and 66.3% on HypOW. On PROB Task 1, it more than doubles the reduction achieved by a K-means

prototype baseline (§5.2).

- **Evaluation: a three-axis framework for post-hoc unknown-stream filters.** Since DualMem leaves the known-class stream untouched, classical WI and A-OSE are structurally insensitive to its main operation. We adopt three complementary axes—FUPI (background-type false-unknown density), UDP (unknown detection precision) (Zhao et al. 2024), and NMH (novel mis-suppression harm)—that together distinguish healthy stream cleanup from aggressive deletion hidden by recall alone.

2 Related Work

Open-world object detection. OWOD extends detection beyond a fixed label space, building on open-set recognition and open-set object detection but adding explicit unknown localization and incremental class learning (Scheirer, Jain, and Boult 2014; Dhamija et al. 2020; Joseph et al. 2021). Methods improve unknown discovery through energy scores (Joseph et al. 2021), attention-driven pseudo-labels (Gupta et al. 2022), probabilistic objectness (Zohar, Wang, and Yeung 2023), hyperbolic embeddings (Doan et al. 2024), unknown-class supervision (Wu et al. 2022), localization-identification cascades (Ma et al. 2023), driving-specific reformulations (Ma et al. 2022), prototype learning (Yu et al. 2022), or training-time objectives on proposal generation (Liang et al. 2023; Wang et al. 2023). All of these determine unknown predictions from *detector-internal* signals. DualMem is orthogonal: it filters the unknown stream of a *frozen* detector with an external critic, requiring no retraining and applicable to proprietary checkpoints.

Open-vocabulary detection and vision-language features. Open-vocabulary detectors use language supervision to recognize categories outside a closed training vocabulary (Gu et al. 2022; Minderer et al. 2022; Cheng et al. 2024). This setting is related but distinct from OWOD: the test-time category names are available, whereas OWOD must flag unknown objects before their labels are introduced. DualMem uses vision-language pretraining only as a frozen proposal critic, not as a classifier over text prompts.

Post-hoc OOD detection. On image classification, post-hoc OOD methods have shown that frozen representations and output scores carry strong OOD signal without modifying the classifier, from maximum-softmax and temperature-scaled baselines to Mahalanobis, energy, and nearest-neighbor scores (Hendrycks and Gimpel 2017; Liang, Li, and Srikant 2018; Lee et al. 2018; Liu et al. 2020; Sun et al. 2022; Park, Jung, and Teoh 2023). We adapt this idea to the proposal level under the OWOD-specific constraint that suppressing OOD-looking predictions must not erase future-task objects. The k -nearest-neighbor construction of our memories is most closely related to KNN-based OOD (Sun et al. 2022), but the dual-memory rule with a positive guard is, to our knowledge, new in this setting.

OWOD evaluation. Traditional metrics—U-Recall, Wilderness Impact, A-OSE (Joseph et al. 2021; Gupta

Detector	Task	Positive U.	Negative U.	Known-as-U.	Ambiguous
PROB	T1	9.1	46.3	23.9	20.8
PROB	T2	7.8	51.9	20.6	19.6
PROB	T3	2.0	52.7	27.3	17.9
PROB	T4	0.0	49.1	33.3	17.6
OW-DETR	T1	2.1	66.9	18.7	12.3
OW-DETR	T2	2.5	63.7	22.0	11.8
OW-DETR	T3	2.4	60.3	25.7	11.6
OW-DETR	T4	0.0	70.6	22.4	6.9
HypOW	T1	9.6	46.2	22.5	21.6
HypOW	T2	6.8	56.6	17.4	19.1
HypOW	T3	1.7	61.2	19.2	17.9
HypOW	T4	0.0	56.0	25.7	18.3

Table 1: Unknown-stream decomposition on M-OWODB. Positive unknowns correspond to future-task objects, negative unknowns correspond to background false positives, known-as-unknown predictions overlap current-known objects, and ambiguous predictions fall outside these clean cases.

et al. 2022; Zohar, Wang, and Yeung 2023)—measure either novel recall or contamination of the known stream. RE-OWOD (Zhao et al. 2024) introduces UDP for unknown precision. We complement UDP with FUPI (absolute background-type false-unknown density) and NMH (false-suppression cost), which together describe the operating space of post-hoc filters operating only on the unknown stream.

3 Why Detector-Internal Filtering Fails

3.1 The Pollution Problem

We first examine what an OWOD detector actually emits in its unknown prediction stream. For each unknown prediction, we assign it to one of four groups by priority. A *positive unknown* is first defined as a prediction with IoU ≥ 0.5 to a future-task ground-truth object. Among the remaining predictions, a *known-as-unknown* prediction overlaps a current-known ground-truth object with IoU ≥ 0.5 . A *negative unknown* has maximum IoU below 0.3 with any ground-truth object, and therefore corresponds to background. The remaining predictions are treated as *ambiguous*, covering intermediate-overlap cases.

Table 1 shows this decomposition across three OWOD detectors and four M-OWODB tasks. The main observation is that positive unknowns form only a small minority of the unknown stream. Across PROB, OW-DETR, and HypOW, all nine detector-task cells from Task 1 to Task 3 contain fewer than 10% positive unknowns. Task 4 contains no future-task objects by construction, so its positive-unknown rate is 0.0%. In contrast, negative unknowns alone account for 46–71% of the stream. This pollution appears across architecturally distinct detectors, suggesting a structural property of detector-internal unknown filtering rather than an idiosyncratic failure of one method.

3.2 The Information Bottleneck

The polluted unknown stream raises a natural question: do OWOD detectors lack the information needed to distinguish

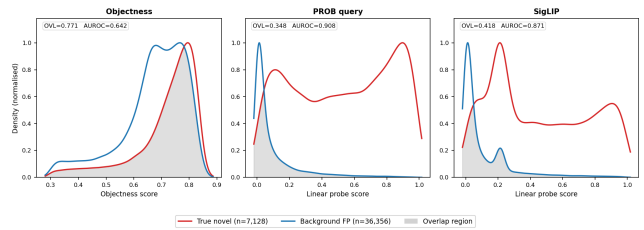


Figure 2: PROB Task 1 feature separability for positive and negative unknown proposals. The objectness score exhibits heavy distribution overlap, whereas the decoder query and frozen SigLIP crop feature provide much stronger separation under a linear probe. Cross-detector quantitative results are reported in Table 2.

positive unknowns from negative unknowns, or is this information present in richer proposal representations but discarded by the final objectness output? We answer this question with a cross-detector binary probing experiment on M-OWODB Task 1. For each detector, we label raw unknown proposals as positive if they match future-task ground truth and negative if they are background false unknowns; known-as-unknown and ambiguous proposals are excluded. We compare three signals: the detector’s final one-dimensional objectness score, a detector-internal proposal feature, and a frozen SigLIP crop feature. Feature representations are evaluated with logistic-regression linear probes under five-fold image-level GroupKFold.

Table 2 shows a consistent pattern across PROB, OW-DETR, and HypOW. The final objectness scalar is weak: objectness AUROC is 0.642 on PROB, 0.526 on OW-DETR, and 0.516 on HypOW, with high positive/negative overlap. In contrast, detector-internal proposal features are strongly discriminative, reaching AUROC 0.908, 0.855, and 0.881, respectively. Frozen SigLIP crop features also retain substantial separability, reaching AUROC 0.871, 0.828, and 0.888.

These results support a cross-detector objectness-bottleneck diagnosis. The unknown stream is not simply devoid of information: richer proposal-level representations, whether internal or external, separate positive and negative unknowns far better than the final scalar objectness output. However, high supervised linear separability does not by itself guarantee that a feature is a good non-parametric memory critic. Section 5.3 shows that, on PROB, the detector query has the highest linear AUROC but is inferior to SigLIP under raw cosine kNN filtering. This motivates DualMem’s use of a frozen external critic whose feature geometry is better aligned with nearest-neighbor retrieval.

This bottleneck is not unique to PROB: the objectness-score overlap coefficient between positive and negative unknowns is 0.771 for PROB, 0.913 for OW-DETR, and 0.952 for HypOW. Detector-output confidence is a weak signal across architectures. The pollution and linear-probe results jointly suggest that the failure is not missing information but *discarded* information at the objectness interface, motivating a post-hoc filter that bypasses this scalar entirely and

Table 2: Cross-detector positive-vs-negative unknown separability on M-OWODB Task 1. The binary labels are positive.unknown = 1 and negative.unknown = 0; known-as-unknown and ambiguous proposals are excluded. AUROC for SigLIP and internal features is measured with five-fold image-level GroupKFold linear probing. OVL is the overlap coefficient of the corresponding one-dimensional score distributions: raw objectness for the objectness column and linear-probe logits for SigLIP and internal features.

Detector	Pos.	Neg.	Obj. AUROC	Obj. OVL	SigLIP AUROC	SigLIP OVL	Internal AUROC	Internal OVL
PROB	7,128	36,356	0.642	0.771	0.871 ± 0.013	0.418	0.908 ± 0.009	0.348
OW-DETR	362	11,757	0.526	0.913	0.828 ± 0.031	0.262	0.855 ± 0.028	0.292
HypOW	4,469	21,412	0.516	0.952	0.888 ± 0.005	0.372	0.881 ± 0.007	0.397

uses frozen external features as an independent critic.

4 DualMem Method

DualMem is a post-hoc filter that bypasses the scalar objectness bottleneck by applying a non-parametric likelihood ratio test in a frozen SigLIP feature space. We describe its three components: a k -nearest-neighbor dual memory (§4.1), a likelihood ratio decision rule (§4.2), and Neyman–Pearson threshold calibration (§4.3).

4.1 Dual k -NN Memory in the SigLIP Feature Space

Calibration assumption. DualMem assumes access to a small image-disjoint calibration split with box-level annotations for held-out future-task objects. These annotations are used only to construct and calibrate the post-hoc filter, and are never used to train or fine-tune the OWOD detector. Thus, our setting should be interpreted as calibrated post-hoc deployment rather than fully annotation-free unknown discovery. In deployment scenarios without annotated novel calibration boxes, one would need to replace M^+ with mined high-confidence object proposals or with a proxy positive memory; we leave this annotation-free variant to future work.

Given a frozen OWOD detector and an image-disjoint calibration split, we collect the detector’s unknown proposals and assign each to one of the four categories defined in Section 3.1. We further split the calibration positives into a memory subset $\mathcal{P}_{\text{mem}}^+$ and a threshold-calibration subset $\mathcal{P}_{\text{thr}}^+$. The positive memory is built only from $\mathcal{P}_{\text{mem}}^+$, while $\mathcal{P}_{\text{thr}}^+$ is reserved for choosing $\tau(\alpha)$. The negative memory $\mathcal{P}_{\text{mem}}^-$ contains background false positives from the calibration split. For each proposal p , we crop the corresponding image region and extract an L_2 -normalized frozen SigLIP ViT-B/16 feature (Dosovitskiy et al. 2021; Zhai et al. 2023), $f(p) \in \mathbb{R}^{768}$.

We define two reference memories directly from these features, with no centroid quantization:

$$M^+ = \{f(p) : p \in \mathcal{P}_{\text{mem}}^+\}, \quad M^- = \{f(p) : p \in \mathcal{P}_{\text{mem}}^-\}. \quad (1)$$

This k -nearest-neighbor construction differs from prototype-based filters (e.g., K -means centroids): every calibration proposal participates in the density estimate, eliminating compression loss at the memory side and following classical k -NN non-parametric density estimation

and its modern use in OOD detection (Loftsgaarden and Quesenberry 1965; Sun et al. 2022). In our experiments, $|\mathcal{M}^-| \approx 30,000$ and $|\mathcal{M}^+|$ ranges from $\sim 0.7\text{K}$ (OW-DETR) to $\sim 8\text{K}$ (PROB) across detectors. We use frozen SigLIP features as the critic; a natural alternative is the detector’s own decoder query, which carries strong supervised separability (AUROC = 0.908, Table 2) but, as we show in §5.3, proves a markedly weaker critic under raw cosine retrieval. We return to this empirical decoupling between supervised AUROC and memory-critic effectiveness in the critic-choice ablation.

4.2 Non-Parametric Likelihood Ratio Test

For a test proposal p , we estimate the class-conditional log-density of $f(p)$ under each memory by a temperature-scaled k -NN kernel estimator:

$$\hat{\ell}^c(p) = \log \sum_{i=1}^k \exp\left(\frac{\cos(f(p), f(p_i^c))}{T}\right) - \log k, \quad (2)$$

where $c \in \{+, -\}$, p_i^c are the top- k nearest neighbors of $f(p)$ in \mathcal{M}^c under cosine similarity, and T is a temperature controlling kernel smoothness. The decision rule is a single-threshold likelihood ratio test:

$$\begin{aligned} \Lambda(p) &= \hat{\ell}^-(p) - \hat{\ell}^+(p), \\ \text{suppress}(p) &= \mathbf{1}[\Lambda(p) > \tau]. \end{aligned} \quad (3)$$

This formulation has two convenient properties. First, as $T \rightarrow 0$, the logsumexp in Eq. 2 reduces to a maximum and $\Lambda(p)$ collapses to a difference of single-prototype cosine similarities; the rule becomes equivalent to a max-cosine positive-guarded suppression. Larger T smooths the kernel and aggregates evidence over multiple neighbors, recovering otherwise brittle decisions on sparse memory regions. Second, the same rule exposes a single, monotonic decision variable $\Lambda(p)$, which makes principled threshold selection possible (§4.3). We use $T = 0.05$ and $k = 25$ as defaults. Moderate changes to T and k did not alter the qualitative ranking of methods.

4.3 Neyman–Pearson Threshold Calibration

A naive choice of τ is a magic number. We instead determine τ on the calibration split using the Neyman–Pearson criterion (Neyman and Pearson 1933): given a user-specified false-suppression budget α on positive unknowns, choose the smallest τ such that

$$\Pr_{p \in \mathcal{P}_{\text{thr}}^+} [\Lambda(p) > \tau] \leq \alpha, \quad (4)$$

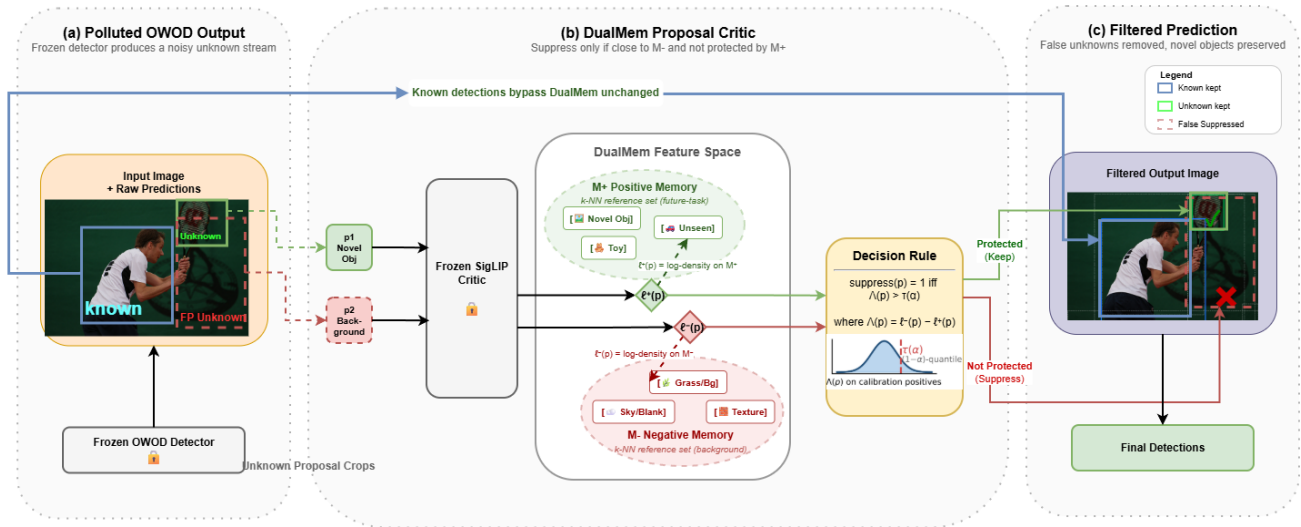


Figure 3: Overview of DualMem. A frozen OWOD detector emits an unknown stream. DualMem crops each unknown proposal, embeds it with a frozen SigLIP critic, compares it against positive and negative k-NN memories, and applies an NP-calibrated likelihood-ratio threshold $\tau(\alpha)$. Known detections bypass the filter entirely.

where $\mathcal{P}_{\text{thr}}^+$ is a hold-out portion of the calibration positives, disjoint from the memories. Operationally, $\tau(\alpha)$ is the $(1-\alpha)$ -quantile of $\{\Lambda(p) : p \in \mathcal{P}_{\text{thr}}^+\}$. This NP-style calibration selects the most aggressive threshold on the calibration positives under a user-specified false-suppression budget. When the k-NN score approximates a likelihood ratio and the calibration and test distributions match, it follows the Neyman–Pearson operating principle; under distribution shift, the realized test-time NMH may deviate from α .

We use $\alpha = 0.10$ throughout the main results. The α -sweep in Section 5.4 shows that the user can trade FUPI for U-Recall in a predictable, monotonic manner. Because the calibration distribution can differ from the test distribution, actual test-time NMH may deviate from α ; in practice we observe $\text{NMH} \leq \alpha$ on PROB and OW-DETR but a positive gap on HypOW (§5.1), which can be mitigated by per-detector validation and, if necessary, a more conservative choice of α .

5 Experiments

Setup. We evaluate DualMem on M-OWODB across three architecturally distinct OWOD detectors: PROB (Zohar, Wang, and Yeung 2023), OW-DETR (Gupta et al. 2022), and HypOW (Doan et al. 2024). Calibration data come from a 20% random subset of COCO train2017 (image-disjoint from val2017); test evaluation is on COCO val2017 following standard OWOD protocol. Unless noted, we use SigLIP ViT-B/16 (Dosovitskiy et al. 2021; Zhai et al. 2023) as the frozen critic, $T = 0.05$, $k = 25$, and $\alpha = 0.10$. All metrics are reported under a unified protocol that scores unknown predictions against future-task ground truth.

A note on classical OWOD metrics. Because DualMem operates only on the unknown stream and leaves known predictions unchanged, the classical WI and A-OSE, which measure unknown contamination in the known-class stream, are structurally insensitive to the main operation of our method. We therefore primarily report FUPI, UDP, NMH, and U-Recall, which directly characterize unknown-stream filtering.

Evaluation labels and metrics. For each detector-emitted unknown prediction d , we compute its IoU with current-task known ground truth G_k and future-task unknown ground truth G_u . We assign proposal labels by the following priority:

$$\ell(d) = \begin{cases} \text{pos}, & \max_{g \in G_u} \text{IoU}(d, g) \geq 0.5, \\ \text{known}, & \max_{g \in G_k} \text{IoU}(d, g) \geq 0.5, \\ \text{neg}, & \max_{g \in G_k \cup G_u} \text{IoU}(d, g) < 0.3, \\ \text{amb}, & \text{otherwise.} \end{cases}$$

Thus, proposals matching future-task objects are treated as positive unknowns; proposals matching current-task objects are known-as-unknown errors; proposals far from all ground truth are background-type negative unknowns; and the remaining intermediate-overlap cases are ambiguous.

Let \mathcal{D} be the raw unknown predictions, $\mathcal{K} \subseteq \mathcal{D}$ the predictions retained after filtering, and \mathcal{I} the evaluation images. We report

$$\text{FUPI} = \frac{|\{d \in \mathcal{K} : \ell(d) = \text{neg}\}|}{|\mathcal{I}|},$$

which measures the number of retained background-type false unknowns per image. FUPI does not include known-



Figure 4: Qualitative success cases on M-OWODB Task 1. Each row pairs raw PROB output (left) with PROB+DualMem (right). Green boxes mark retained novel proposals, red boxes retained background false positives, and dashed white boxes background proposals suppressed by DualMem. Across these scenes, DualMem removes 6–12 background false positives per image while suppressing zero positive unknowns.

as-unknown predictions. The suppression gain is

$$SG = 1 - \frac{|\{d \in \mathcal{K} : \ell(d) = \text{neg}\}|}{|\{d \in \mathcal{D} : \ell(d) = \text{neg}\}|}.$$

Novel mis-suppression harm is proposal-level:

$$NMH = \frac{|\{d \in \mathcal{D} \setminus \mathcal{K} : \ell(d) = \text{pos}\}|}{|\{d \in \mathcal{D} : \ell(d) = \text{pos}\}|}.$$

For standard OWO metrics, we follow prior definitions: U-Recall is computed as in OWO (Dosovitskiy et al. 2021), and UDP follows RE-OWO (Zhao et al. 2024). For raw detectors we evaluate these metrics on the original unknown stream \mathcal{D} ; for post-hoc filters we evaluate them on the retained stream \mathcal{K} after suppression. Thus, FUPI and NMH are newly introduced proposal-level diagnostics, whereas U-Recall and UDP are inherited metrics reported under the same retained-output protocol.

5.1 Main Results

Table 3 reports DualMem across three OWO detectors on M-OWODB Task 1. DualMem reduces FUPI substantially on all three detectors: by 58.6% on PROB (7.35 \rightarrow 3.04), 44.9% on OW-DETR (2.83 \rightarrow 1.56), and 66.3% on HypOW (5.23 \rightarrow 1.76). UDP improves correspondingly, from 0.114 \rightarrow 0.258 on PROB, 0.023 \rightarrow 0.042 on OW-DETR,

Method	Detector	FUPI \downarrow	UDP \uparrow	NMH	U-Recall	Δ U-Rec.
Raw	PROB	7.35	0.114	–	0.218	–
+ DualMem	PROB	3.04	0.258	6.4%	0.206	–1.2
Raw	OW-DETR	2.83	0.023	–	0.020	–
+ DualMem	OW-DETR	1.56	0.042	7.5%	0.018	–0.2
Raw	HypOW	5.23	0.123	–	0.179	–
+ DualMem	HypOW	1.76	0.270	22.6%	0.145	–3.4
Mean reduction	–	–56.6%	+119.2%	–	–	–1.6 pp

Table 3: Main results on M-OWODB Task 1. DualMem substantially reduces background-type false-unknown density and improves UDP across three detectors at $\alpha = 0.10$. NMH stays close to the calibration target on PROB and OW-DETR; on HypOW it exceeds the target, indicating a calibration–test mismatch and the need for per-detector validation.

and 0.123 \rightarrow 0.270 on HypOW. The mean FUPI reduction across the three detectors is 56.6%. On PROB Task 1, DualMem achieves a 58.6% FUPI reduction, more than doubling the 24.5% reduction achieved by the K-means prototype baseline (Table 4).

NMH remains close to the calibration target $\alpha = 0.10$ on PROB (6.4%) and OW-DETR (7.5%). On HypOW, actual NMH (22.6%) exceeds the target. We attribute this gap to a distribution mismatch between HypOW’s positive unknowns—which concentrate near low-density regions in SigLIP space—and the calibration positives used for quantile selection. The NP framework makes this case explicit and addressable: using a more conservative α on HypOW can reduce the realized NMH, but requires per-detector validation. Crucially, because DualMem is applied only to predictions assigned to the unknown stream and known-class predictions bypass the filter, known-class mAP is unchanged under the standard evaluation pipeline. Figure 4 shows four representative scenes in which DualMem removes 6–12 background false positives per image while preserving all positive unknowns—a visual counterpart to the FUPI and NMH numbers in Table 3.

5.2 Why Dual Memory? Ablation

Table 4 compares DualMem with two baselines on PROB Task 1: a tuned objectness threshold, and a *KMeans prototype baseline* that compresses each memory into K centroids and uses a max-cosine dual-threshold rule (\mathcal{M}^+ : $K=16$; \mathcal{M}^- : $K=64$; $\tau=0.80$). This baseline isolates the contribution of our three design choices— k -NN reference set, LRT smoothing, NP calibration—against a natural prototype-compression alternative. The upgraded DualMem achieves a 45.2% lower FUPI than the prototype baseline (5.55 \rightarrow 3.04) while *simultaneously* reducing NMH (7.4% \rightarrow 6.4%). Compared with objectness thresholding, DualMem reaches a much lower FUPI (3.04 vs. 5.85) at less than half the NMH (6.4% vs. 13.7%). The improvement decomposes as follows: replacing KMeans centroids with the full k -NN reference set is the dominant gain (FUPI 5.55 \rightarrow 3.12 at $T \rightarrow 0$, –43.6%); LRT temperature smoothing with $T = 0.05$ provides additional refinement (3.12 \rightarrow 3.04, –2.6% relative);

Strategy	FUPI↓	NMH↓	U-Recall	UDP↑
Raw PROB	7.35	–	0.218	0.114
+ Objectness threshold (≥ 0.60)	5.85	13.7%	0.204	0.139
+ KMeans prototype baseline ($\tau=0.80$)	5.55	7.4%	0.207	0.150
+ DualMem (LRT+kNN+NP, $\alpha=0.10$)	3.04	6.4%	0.206	0.258

Table 4: Decision-rule ablation on PROB Task 1. The upgraded DualMem improves on both the KMeans prototype baseline and a tuned objectness threshold in FUPI and NMH simultaneously.

and NP calibration replaces a magic threshold with an explicit, monotonic α -controlled trade-off.

5.3 Critic Choice

Table 5 compares frozen critics on PROB Task 1 under the upgraded framework. The most striking observation concerns the detector’s own decoder query: *despite the highest linear-probe AUROC of all tested features* (0.908; Table 2), it is the *worst* single critic under memory-based retrieval (FUPI 3.40, NMH 10.2%). DINOv2 shows the same pattern in a milder form: a slightly higher linear-probe AUROC than SigLIP (0.879 vs. 0.871, not shown in the table), but a higher NMH (8.2% vs. 6.4%) under cosine k -NN retrieval (Oquab et al. 2024). This is a direct empirical decoupling: AUROC measures separability *after* an optimal supervised one-dimensional projection, while DualMem relies on the *raw* geometry of the feature space. PROB’s decoder query encodes detection-specific spatial and class information shaped by the DETR training objective (Carion et al. 2020); its raw cosine structure carries discriminative signal only after a learned projection. By contrast, CLIP/SigLIP-style language–image pretraining aligns semantic similarity with feature-space geometry (Radford et al. 2021; Zhai et al. 2023), yielding a feature space in which k -NN retrieval directly captures object identity.

Among the single critics, SigLIP achieves the best NMH (6.4%, closest to the calibration target $\alpha = 0.10$) and the highest U-Recall (0.206), at a modest FUPI cost (3.04 vs. 2.88 for DINOv2). We adopt SigLIP as the default. Fused critics (SigLIP||PROB concat, SigLIP+PROB average) reduce FUPI further to 2.35 but at the cost of higher dimensionality (1024-D / averaged 256-D) and higher NMH; we report these for completeness but do not use them as the default. CLIP ViT-B/32 (Radford et al. 2021) yields the lowest FUPI (1.53) but with 24.8% NMH, suppressing one in four positive unknowns and dropping U-Recall by 5pp—a clear case where aggressive false-positive cleanup overrides the NP budget, and a useful negative example of how a misaligned critic geometry can subvert the calibration framework.

Implication. The decoupling between linear-probe AUROC and memory-based filtering effectiveness has a practical consequence: *the natural-looking idea of using the detector’s internal decoder query as a critic does not work*, even though the information is provably there (AUROC = 0.908). Recovering this information requires a feature space whose raw geometry is aligned with semantic similarity—

Critic feature	Dim.	FUPI↓	UDP↑	NMH↓	U-Recall
Raw PROB	–	7.35	0.114	–	0.218
PROB decoder query	256	3.40	0.204	10.2%	0.206
DINOv2 ViT-B/14	768	2.88	0.268	8.2%	0.205
SigLIP ViT-B/16	768	3.04	0.258	6.4%	0.206
SigLIP + PROB (avg)	256	2.35	0.303	9.2%	0.205
SigLIP PROB (concat)	1024	2.35	0.305	7.1%	0.206
CLIP ViT-B/32	512	1.53	0.303	24.8%	0.168

Table 5: Critic ablation on PROB Task 1 under the LRT+kNN+NP framework. SigLIP achieves the best NMH and the highest U-Recall, and is used as the default critic. CLIP yields lower FUPI but higher NMH (24.8%); we report it as a stress test, not as a recommendation.

which is precisely what a contrastively pretrained external critic provides, and what the detector’s training objective does not. This complements our main information-bottleneck thesis: the loss at the objectness head is not the only structural problem; the decoder query itself, while information-rich, is geometrically unsuited for the post-hoc critic role.

5.4 User-Controllable Trade-off: α Sweep

A key advantage of the NP framework is that τ is no longer a magic constant. Figure 5 shows the α sweep on PROB Task 1: α monotonically trades FUPI for U-Recall, and actual NMH on the test split is consistently *below* the target budget on PROB, reflecting a conservative (user-favorable) calibration gap. Users can pick an operating point matching their downstream tolerance for novel mis-suppression—e.g., $\alpha = 0.05$ yields NMH = 2.9% at the cost of higher FUPI (3.90), while $\alpha = 0.20$ pushes FUPI down to 2.26 at NMH = 13.7%.

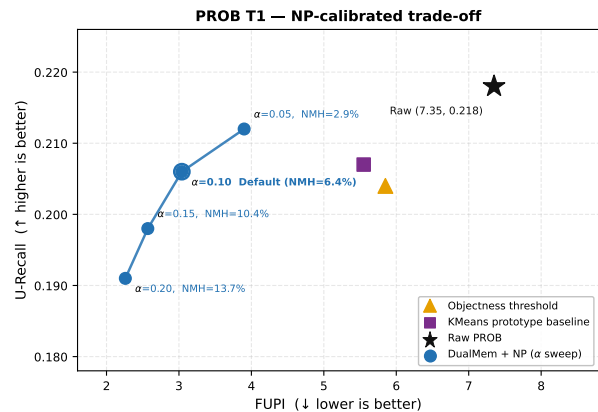


Figure 5: NP-calibrated α sweep on PROB Task 1. Each operating point corresponds to a user-specified false-suppression budget α . The curve monotonically traces a precision–recall trade-off; the raw detector and a tuned objectness threshold are shown for reference. The default $\alpha = 0.10$ is marked.

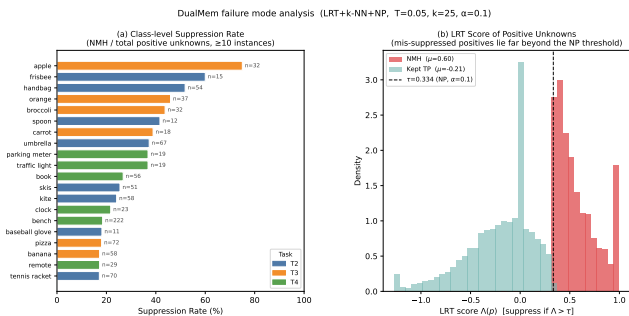


Figure 6: Failure analysis of DualMem on positive unknown proposals under the default LRT+kNN+NP configuration ($T = 0.05$, $k = 25$, $\alpha = 0.10$). (a) Mis-suppression is class-concentrated rather than uniform; only classes with at least ten positive unknown proposals are shown; rates for low-count classes should be interpreted as descriptive rather than statistically stable. (b) Mis-suppressed positives have substantially higher LRT scores than retained true-positive unknowns and lie beyond the NP-calibrated threshold, indicating that most failures are not marginal boundary cases.

6 Discussion and Limitations

DualMem is a post-hoc filter, not a replacement for training-time OWO objectives. Some methods directly suppress false unknowns during training (e.g., UnSniffer (Liang et al. 2023)); applying DualMem on top of such a detector yields near-zero additional gain, indicating that the two regimes target overlapping failure modes. DualMem is most useful when the detector is fixed: proprietary checkpoints, large pretrained OWO models, or legacy detectors. In this setting, the frozen external critic recovers information that the detector’s one-dimensional unknown confidence does not expose.

Detector-internal residual. A natural extension is to add a trained residual head $g_\theta(q(p))$ on top of $\Lambda(p)$, where $q(p)$ is the detector’s 256-D decoder query. On PROB Task 1, this yields negligible additional gain (FUPI 3.04 \rightarrow 3.03, $< 1\%$). We interpret this—together with its lack of cross-detector applicability—as further evidence for the information-bottleneck thesis: the detector-internal signal and the SigLIP signal recover overlapping discriminative content, and stacking them does not produce additive gains. We therefore exclude the residual head from the main DualMem configuration.

Failure analysis. Figure 6 analyzes positive unknown proposals suppressed by DualMem on PROB. Mis-suppression is not uniformly distributed across classes: several visually context-dependent categories, such as apple, frisbee, handbag, orange, and broccoli, exhibit substantially higher suppression rates. In the decision space, mis-suppressed positives are shifted well beyond the NP threshold, whereas retained positives concentrate mostly below it. This suggests that DualMem failures are not merely boundary cases, but arise when true novel objects are represented as background-like under the frozen critic geometry.

Limitations. We note three. (i) The NP budget does not transfer uniformly across detectors: PROB and OW-DETR stay near the target, whereas HypOW exhibits a larger calibration–test gap. (ii) As shown in Fig. 6, suppressed positives are concentrated in a small set of visually context-dependent categories, and their LRT scores lie well beyond the NP threshold. This points to a limitation of the frozen critic geometry rather than objectness alone. (iii) DualMem relies on a small annotated calibration split to build the positive memory M^+ . This is weaker than retraining the detector on future classes, since detector parameters remain frozen, but it is not a fully annotation-free OWO setting. The method is therefore most appropriate for calibrated post-hoc deployment, auditing, or model maintenance scenarios where a small set of novel-object annotations is available.

7 Conclusion

OWO detectors expose a weak scalar interface for unknown detection: across PROB, OW-DETR, and HypOW, the final objectness score is a poor positive-vs-negative unknown discriminator, whereas detector-internal proposal features and frozen SigLIP crop features retain substantially stronger separability. This identifies a cross-detector objectness bottleneck: discriminative proposal-level information exists, but is not reliably exposed by the final one-dimensional unknown confidence.

DualMem addresses this bottleneck as a calibrated post-hoc filter. It performs a non-parametric likelihood-ratio test in frozen SigLIP feature space using positive and negative k-nearest-neighbor memories, and selects the suppression threshold through Neyman–Pearson calibration. Across PROB, OW-DETR, and HypOW on M-OWODB Task 1, DualMem reduces background false unknown density by 44.9–66.3% (mean 56.6%) while keeping U-Recall within 3.4 percentage points; known-class mAP is unchanged because known detections bypass the filter. These results suggest that post-hoc unknown-stream cleanup is a useful complement to training-time OWO objectives, especially when the detector is fixed.

References

- Carion, N.; Massa, F.; Synnaeve, G.; Usunier, N.; Kirillov, A.; and Zagoruyko, S. 2020. End-to-End Object Detection with Transformers. In *Proceedings of the European Conference on Computer Vision*, 213–229.
- Cheng, T.; Song, L.; Ge, Y.; Liu, W.; Wang, X.; and Shan, Y. 2024. YOLO-World: Real-Time Open-Vocabulary Object Detection. In *Proceedings of the IEEE/CVF Conference on Computer Vision and Pattern Recognition*, 16901–16911.
- Dhamija, A. R.; Günther, M.; Ventura, J.; and Boulton, T. E. 2020. The Overlooked Elephant of Object Detection: Open Set. In *Proceedings of the IEEE/CVF Winter Conference on Applications of Computer Vision*, 1010–1019.
- Doan, T.; Li, X.; Behpour, S.; He, W.; Gou, L.; and Ren, L. 2024. Hyp-OW: Exploiting Hierarchical Structure Learning with Hyperbolic Distance Enhances Open World Object Detection. In *Proceedings of the AAAI Conference on Artificial Intelligence*, volume 38, 1555–1563.

- Dosovitskiy, A.; Beyer, L.; Kolesnikov, A.; Weissenborn, D.; Zhai, X.; Unterthiner, T.; Dehghani, M.; Minderer, M.; Heigold, G.; Gelly, S.; Uszkoreit, J.; and Hounsby, N. 2021. An Image is Worth 16x16 Words: Transformers for Image Recognition at Scale. In *Proceedings of the International Conference on Learning Representations*.
- Gu, X.; Lin, T.-Y.; Kuo, W.; and Cui, Y. 2022. Open-Vocabulary Object Detection via Vision and Language Knowledge Distillation. In *Proceedings of the International Conference on Learning Representations*.
- Gupta, A.; Narayan, S.; Joseph, K. J.; Khan, S.; Khan, F. S.; and Shah, M. 2022. OW-DETR: Open-World Detection Transformer. In *Proceedings of the IEEE/CVF Conference on Computer Vision and Pattern Recognition*, 9235–9244.
- Hendrycks, D.; and Gimpel, K. 2017. A Baseline for Detecting Misclassified and Out-of-Distribution Examples in Neural Networks. In *Proceedings of the International Conference on Learning Representations*.
- Joseph, K. J.; Khan, S.; Khan, F. S.; and Balasubramanian, V. N. 2021. Towards Open World Object Detection. In *Proceedings of the IEEE/CVF Conference on Computer Vision and Pattern Recognition*, 5830–5840.
- Lee, K.; Lee, K.; Lee, H.; and Shin, J. 2018. A Simple Unified Framework for Detecting Out-of-Distribution Samples and Adversarial Attacks. In *Advances in Neural Information Processing Systems*.
- Liang, S.; Li, Y.; and Srikant, R. 2018. Enhancing the Reliability of Out-of-Distribution Image Detection in Neural Networks. In *Proceedings of the International Conference on Learning Representations*.
- Liang, W.; Xue, F.; Liu, Y.; Zhong, G.; and Ming, A. 2023. Unknown Sniffer for Object Detection: Don't Turn a Blind Eye to Unknown Objects. In *Proceedings of the IEEE/CVF Conference on Computer Vision and Pattern Recognition*, 3230–3239.
- Liu, W.; Wang, X.; Owens, J. D.; and Li, Y. 2020. Energy-Based Out-of-Distribution Detection. In *Advances in Neural Information Processing Systems*.
- Loftsgaarden, D. O.; and Quesenberry, C. P. 1965. A Non-parametric Estimate of a Multivariate Density Function. *The Annals of Mathematical Statistics*, 36(3): 1049–1051.
- Ma, S.; Wang, Y.; Wei, Y.; Fan, J.; Li, T. H.; Liu, H.; and Lv, F. 2023. CAT: LoCalization and IdentificAtion Cascade Detection Transformer for Open-World Object Detection. In *Proceedings of the IEEE/CVF Conference on Computer Vision and Pattern Recognition*, 19681–19690.
- Ma, Z.; Yang, Y.; Wang, G.; Xu, X.; Shen, H. T.; and Zhang, M. 2022. Rethinking Open-World Object Detection in Autonomous Driving Scenarios. In *Proceedings of the ACM International Conference on Multimedia*, 1279–1288.
- Minderer, M.; Gritsenko, A. A.; Stone, A.; Neumann, M.; Weissenborn, D.; Dosovitskiy, A.; Mahendran, A.; Arnab, A.; Dehghani, M.; Shen, Z.; Wang, X.; Zhai, X.; Kipf, T.; and Hounsby, N. 2022. Simple Open-Vocabulary Object Detection. In *Proceedings of the European Conference on Computer Vision*, 728–755.
- Neyman, J.; and Pearson, E. S. 1933. On the Problem of the Most Efficient Tests of Statistical Hypotheses. *Philosophical Transactions of the Royal Society of London. Series A*, 231(694–706): 289–337.
- Oquab, M.; Darcet, T.; Moutakanni, T.; Vo, H. V.; Szafraniec, M.; Khalidov, V.; Fernandez, P.; Haziza, D.; Massa, F.; El-Nouby, A.; Assran, M.; Ballas, N.; Galuba, W.; Howes, R.; Huang, P.-Y.; Li, S.-W.; Misra, I.; Rabbat, M.; Sharma, V.; Synnaeve, G.; Xu, H.; Jegou, H.; Mairal, J.; Labatut, P.; Joulin, A.; and Bojanowski, P. 2024. DI-NOv2: Learning Robust Visual Features without Supervision. *Transactions on Machine Learning Research*.
- Park, J.; Jung, S.; and Teoh, A. B. J. 2023. Nearest Neighbor Guidance for Out-of-Distribution Detection. In *Proceedings of the IEEE/CVF International Conference on Computer Vision*.
- Radford, A.; Kim, J. W.; Hallacy, C.; Ramesh, A.; Goh, G.; Agarwal, S.; Sastry, G.; Askell, A.; Mishkin, P.; Clark, J.; Krueger, G.; and Sutskever, I. 2021. Learning Transferable Visual Models From Natural Language Supervision. In *Proceedings of the International Conference on Machine Learning*, 8748–8763.
- Scheirer, W. J.; Jain, L. P.; and Boulton, T. E. 2014. Probability Models for Open Set Recognition. *IEEE Transactions on Pattern Analysis and Machine Intelligence*, 36(11): 2317–2324.
- Sun, Y.; Ming, Y.; Zhu, X.; and Li, Y. 2022. Out-of-Distribution Detection with Deep Nearest Neighbors. In *Proceedings of the International Conference on Machine Learning*.
- Wang, Y.; Yue, Z.; Hua, X.-S.; and Zhang, H. 2023. Random Boxes Are Open-world Object Detectors. In *Proceedings of the IEEE/CVF International Conference on Computer Vision*, 6233–6243.
- Wu, Z.; Lu, Y.; Chen, X.; Wu, Z.; Kang, L.; and Yu, J. 2022. UC-OWOD: Unknown-Classified Open World Object Detection. In *Proceedings of the European Conference on Computer Vision*, 193–210.
- Yu, J.; Ma, L.; Li, Z.; Peng, Y.; and Xie, S. 2022. Open-World Object Detection via Discriminative Class Prototype Learning. In *Proceedings of the IEEE International Conference on Image Processing*, 626–630.
- Zhai, X.; Mustafa, B.; Kolesnikov, A.; and Beyer, L. 2023. Sigmoid Loss for Language Image Pre-Training. In *Proceedings of the IEEE/CVF International Conference on Computer Vision*, 11941–11952.
- Zhao, X.; Liu, X.; Shen, Y.; Qiao, Y.; Ma, Y.; and Wang, D. 2024. Revisiting Open World Object Detection. *IEEE Transactions on Circuits and Systems for Video Technology*, 34(5): 3496–3509.
- Zohar, O.; Wang, K.-C.; and Yeung, S. 2023. PROB: Probabilistic Objectness for Open World Object Detection. In *Proceedings of the IEEE/CVF Conference on Computer Vision and Pattern Recognition*, 11444–11453.